



LAWRENCE
LIVERMORE
NATIONAL
LABORATORY

Fracture Permeability Evolution in Rock from the Desert Peak EGS Site

Steven R. Carlson, Jeffery J. Roberts, Russel L.
Detwiler, Elizabeth A. Burton, Ann Robertson-Tait,
Christy Morris, Paul Kasameyer

April 15, 2004

Geothermal Resources Council Annual Meeting
Palm Springs, CA, United States
August 29, 2004 through September 1, 2004

Disclaimer

This document was prepared as an account of work sponsored by an agency of the United States Government. Neither the United States Government nor the University of California nor any of their employees, makes any warranty, express or implied, or assumes any legal liability or responsibility for the accuracy, completeness, or usefulness of any information, apparatus, product, or process disclosed, or represents that its use would not infringe privately owned rights. Reference herein to any specific commercial product, process, or service by trade name, trademark, manufacturer, or otherwise, does not necessarily constitute or imply its endorsement, recommendation, or favoring by the United States Government or the University of California. The views and opinions of authors expressed herein do not necessarily state or reflect those of the United States Government or the University of California, and shall not be used for advertising or product endorsement purposes.

Fracture Permeability Evolution in Rock from the Desert Peak EGS Site

**Steven R. Carlson¹, Jeffery J. Roberts¹, Russell L. Detwiler¹, Elizabeth A. Burton¹,
Ann Robertson-Tait², Christy Morris², Paul Kasameyer¹**

¹Lawrence Livermore National Laboratory, Livermore, California

²GeothermEx, Inc., Richmond, California

³ORMAT Nevada Inc., Reno, Nevada

Abstract

Fluid flow experiments are being conducted on core specimens of quartz monzonite retrieved from depths of about 1 km at the Desert Peak East EGS site in Churchill County, Nevada. Our immediate goal is to observe permeability evolution in fractures at pressure and temperature conditions appropriate to the Desert Peak geothermal site. Longer term, we aim to evaluate mechanisms that control the evolution of fracture permeability. In the experiments saline water is flowed through an artificial fracture at a constant rate of 0.02 ml/min over a period of several weeks. The constant flow tests are interrupted at selected times for shorter tests in which flow is either stopped or varied between 0 and 2.0 ml/min. The experiments to date were conducted at a confining pressure of 5.5 MPa, pore pressures of 1.38 MPa or 2.07 MPa and temperatures of 167-169°C. Measurements include differential pressure and electrical resistance across the specimen. The short-term variable flow rate experiments allow us to calculate the effective hydraulic aperture of the fracture at various times during the experiment. Changes in electrical resistivity provide indirect evidence of ongoing mineral dissolution and precipitation processes that are expected to change fracture permeability over time. The early experiments have shown that electrical resistivity rises during flow and falls during intervals in which flow is stopped.

Introduction

The development of Enhanced Geothermal Systems (EGS) depends on the creation of permeable fractures. Once fractures are created, the success of the program depends on choosing appropriate operational procedures to maintain and enhance permeability in order to extract heat from the fractured rock. These operational procedures will depend on and be influenced by many mechanisms that cause changes in fracture permeability with time. Mechanisms include dissolution and precipitation caused by temperature differences, chemistry effects, flow rates and stress environment (e.g., Polak et al., 2003). An effective EGS program will require the ability to predict the evolution of fracture permeability with time, and to evaluate alternative operational strategies for maintaining and enhancing fracture permeability. Our goal is to evaluate some of these mechanisms and strategies by performing fracture permeability evolution experiments and modeling on rocks from the Desert Peak EGS site.

Carlson, Roberts and Detwiler

Figure 1 shows a schematic picture of the flow due to injection into a fracture zone. At any time, fluid is moving along flow lines, and chemical and thermal fronts are moving in the same direction at a slower rate than the fluid. Thermal, chemical and mechanical phenomena will produce changes in fracture permeability and fluid flow patterns. Quantitative prediction of the evolution of fracture permeability will require numerical models. There are several models available or being developed to model phenomena in coupled thermal, chemical and mechanical systems. (NUFT, Tetrad, TOUGH React) Given accurate information about how the fluid and rock interact within a small element, these models will attempt to predict changes in local permeability, modifications of flow paths through a fracture and the effective reduction or increase of system permeability and heat extraction with time. Unfortunately, there is a paucity of hard information about the parameters that describe the behavior of a single element in these codes. Determining the critical parameters needed to predict the evolution of fracture permeability is a large task and will depend on many variables including rock type, fluid chemistry, injectate and reservoir temperatures, local stress field, fracture strain rate, and the proximity of natural fractures to the well bore.

EGS schematic here (Figure 1).

We have initiated an effort to determine these parameters for samples from the Desert Peak EGS project. The work consists of performing laboratory experiments designed to assess the evolution of permeability and geochemical attributes of induced fractures in geothermal environments under a few sets of expected conditions within the engineered reservoir, and using geochemical modeling to extrapolate those results to a broader range of expected conditions. LLNL has developed a laboratory system to measure electrical properties and permeability of core samples under a controlled stress environment at temperatures up to 200°C and pressures up to 1500 psi. This system has been used to identify resistivity signatures of boiling in intact and fractured samples from geothermal fields (Detwiler *et al*, 2003). That system has been modified to measure permeability and differential pressure and will be combined with geochemical modeling and chemical analyses of the fluid in order to assess permeability evolution quantitatively on artificial and natural fractures in geothermal core as a function of effective stress, fluid chemistry, and temperature. The short-term goal of these experiments is to separate the physical and chemical effects that lead to fracture permeability evolution, and to identify conditions under which permeability will be enhanced or reduced. The long-term goal is to provide quantitative input for parameters of coupled codes to model the evolution of fracture permeability. In this paper, we report initial experiments on core from the Desert Peak EGS site.

Background

The Desert Peak East EGS Project is an industry-DOE sponsored effort to investigate the technical feasibility of creating an artificial geothermal reservoir east of the Desert Peak geothermal field in the Hot Springs Mountains, Churchill County, Nevada. An overview

of the project is provided in Robertson-Tait and Morris (2003). Current plans are to stimulate a hot, tight hole (DP 23-1) east of the producing wells at Desert Peak. The hydraulic stimulation effort is supported by injection tests (Sanyal *et al.*, 2003), a detailed borehole fracture analysis (Robertson-Tait *et al.*, 2004) and mechanical and other tests on core specimens retrieved from hole 35-13 TCH located 2.4 km (1.5 mi) northeast of borehole DP 23-1.

Test Specimens

The sample materials were retrieved from depths of 1194 m (3916 feet) and 1210 m (3972 feet) from borehole 35-13 TCH. They consist of quartz monzonite, composed of 44% plagioclase, 23% potassium feldspar, 7% quartz and 3% mica (Lutz, 2003). The rock contains numerous, sealed fractures in-filled with secondary minerals such as kaolin (6%), calcite (4%), and dolomite (4%). Sample porosities, calculated from the dry and saturated specimen weights, are about 2%. This value is likely an upper bound on the porosity as the measurements include any microcracks that were induced by cooling and the release of stress upon retrieval from depth. A more complete geologic description of rock samples from boreholes DP 23-1 and 13-35 TCH is provided by Lutz *et al.* (2003).

Flow measurements in these experiments are made through artificial fractures. The fractures are prepared by cutting sections of the core along the long axis with a Mettler AE240 water-cooled rock saw. The sections are fitted back together, and two sub-cores, centered over the saw-cut, are bored from each section. The sub-cores comprise a pair of right circular cylinders, 25.4 mm in diameter and 43.2 mm in length, bisected by a planar saw-cut. The specimen half-cylinders are labeled A and B. The fracture surface labeled B is then bead blasted using 70-140 grit glass beads, and the other surface is hand lapped with 320-400 grit.

The fracture surfaces are photographed with an optical microscope at 6.3x and 20x, and portions of specimen 3972.2A were imaged with a scanning electron microscope. The specimens contain numerous sealed fractures, one of which can be seen in Figure 2.

Fracture surface optical microscope photo here (Figure 2).

A vacuum saturation technique is used to saturate the specimens with a dilute saline solution similar in salinity to the produced reservoir fluid. Planned experiments include a more complicated injectate including silica.

Experimental Procedures

Experimental Apparatus

The test specimens are jacketed in 1-mm thick Viton tubing and fitted with Hastelloy C endcaps (Figure 3). The inlet endcap contains a narrow reservoir designed to distribute

fluid uniformly along the upstream edge of the fracture. Care is taken to align the reservoir with the fracture. The outlet endcap contains a series of concentric channels to collect fluid over the entire surface at the downstream specimen end. Two perforated platinum disks contact the ends of the cylindrical test specimen and serve as electrodes. Thin mica inserts provide electrical insulation between the endcaps and a mounting frame that provides a small end load to the sample.

Fig. 3. Detail of pressure vessel/specimen assembly.

The test specimen is inserted into an externally heated, hydrostatic pressure vessel (Figure 4). Dow Syltherm 800 heat transfer fluid is used as the confining medium. Confining pressure is supplied by an APCS pump and measured with a pressure transducer. Temperature is controlled by using three Yokogawa temperature controllers that control four resistance heaters placed on the outside of the pressure vessel. Confining fluid temperature is measured by a type-T thermocouple near the test specimen. The pore fluid lines are 1.59 mm diameter Hastelloy tubing. The inlet line is arranged in a spiral to allow the upstream fluid to attain the same temperature as the rock specimen before entering the fracture. Fluid enters the specimen at the lower end and flows upward through the fracture.

Fig. 4. Overall view of test apparatus and data acquisition system.

Pore fluid is prepared by adding 8.5g/l of high-purity NaCl to distilled water. The solution has an electrical conductivity of 13.75 mS/cm at room temperature. The saline solution is de-aerated for approximately 20 minutes before being introduced into the upstream reservoir. The pore fluid supply is controlled by two Isco 500D syringe pumps capable of controlling either fluid pressure or flow rate. The upstream and downstream pore fluid pressures are measured individually, and the pressure difference between the upstream and downstream reservoirs is measured with a Validyne model DP 215-50 differential pressure transducer. A second, identical differential pressure transducer monitors ambient air pressure. A single specimen, DP 3916, was tested before the Validyne differential pressure transducers were added to the system.

The pressure transducer and temperature voltages are read with an Agilent 34970A digital multimeter. Resistance measurements are made at 1 kHz with an HP 4284 LCR meter. Data acquisition is controlled by National Instruments LabVIEW software on an Apple microcomputer. The APCS and Isco syringe pumps are also under computer control.

Procedures

Flow tests are conducted at constant temperatures and confining pressures. All tests to date have used a confining pressure of 5.5 MPa (800 psi) and a temperature of 167-169°C (333°F). In the usual mode of operation, the downstream syringe pump is set to control

fluid pressure at a fixed value, and the upstream syringe pump is set to control flow rate at 0.02 ml/min. A pore pressure of 1.38 MPa (200 psi) was used for specimen DP 3916 and 2.07 MPa (300 psi) was used for DP 3972.2. When configured in this manner the pore-pressure pumps provide a constant pore pressure at the downstream end and a constant flow rate through the fracture. The upstream syringe pump continually adjusts pressure to maintain a constant flow rate and the pressure difference across the specimen is measured. Changes in differential pressure across the specimen thus provide evidence of permeability change in the fracture over time.

At selected times we calculate the effective hydraulic aperture of our specimen based on the relationship for flow between two parallel surfaces. To do this, flow rates are varied from 0.0 to 2.0 ml/min and differential pressures are recorded over five minute intervals at each flow rate. The differential pressures are divided by the specimen length to give pressure gradients. The flow rates are plotted against pressure gradients, and the slope of the linear portion of the plot is used to calculate effective hydraulic aperture, b , as

$$b^3 = 12\mu QL/(W\Delta P) \quad (1)$$

where μ is the dynamic viscosity of water, Q is the volumetric flow rate, W and L are the fracture width and length, respectively, and ΔP is the pressure difference across the specimen. The dynamic viscosity of water at 167°C and 2.0 MPa pressure is obtained by linear interpolation of tabulated data given in Clarke (1966). The Reynolds number, Re , is calculated as

$$Re = Vb\rho/\mu \quad (2)$$

where V is the average fluid velocity (flow rate/cross-sectional area) and ρ is density. As before, b is the effective hydraulic aperture and μ is dynamic viscosity.

Flow is interrupted at selected times so that changes in electrical resistance can be monitored under no-flow conditions over periods of up to six days. Electrical resistance is strongly sensitive to the presence of dissolved ions in the pore fluid. Observed changes in resistance over time provide evidence for active mineral dissolution and precipitation processes in the fracture. The resistance data are converted to resistivity and fit to kinetic equations using *TableCurve2D*, a commercially available curve-fitting application. Electrical resistivity is calculated from the measured resistances and the specimen geometry.

Results and Discussion

Fracture permeability

We have completed experiments on two samples thus far, DP 3916 and DP 3972.2, and testing of a third specimen, DP 3972.1, is underway. The experiments have met with

mixed success, but they have provided valuable information used in the experimental design and test protocol. Sample DP 3916 served as the initial shakedown experiment, lasting 44 days (41 days of flow) before jacket failure. Differential pressure measurements were not made on specimen DP 3916.

No upward or downward trend was observed over time in the differential pore pressure data for specimen DP 3972.2 prior to jacket failure after 38 days. Based on the scatter in the DP 3972.2 data we expect to resolve differential pressure changes of 0.14 kPa (0.02 psi). By rearranging the terms in equation (1) to solve for ΔP and substituting in the appropriate values for the various parameters, it can be seen that only very small changes in the pressure differential can be expected for aperture changes of a few microns at an initial fracture aperture of about 20 μm (Table 1). Future experiments will need to utilize a more sensitive pressure transducer or involve modifications to our specimen preparation or other experimental procedures to bring about a larger pressure response.

Figure 5. Flow vs. Pressure Gradient

Much better results were obtained in our efforts to measure effective hydraulic aperture by varying fluid flow rates. The flow rates are plotted against pressure gradients in Figure 5 and a linear relationship is observed to about 0.2 ml/min. A line was fit to the linear portion of the data using ordinary least squares (Figure 6). An effective hydraulic aperture of 18.5 μm was calculated from equation (1) from the slope of the regression line, the specimen dimensions and a value of 1.86×10^{-4} Pa-s for the dynamic viscosity of water at 167°C and 2.0 MPa (Clarke, 1966). A Reynolds number of 0.64 was calculated at the 0.2 ml/min flow rate using equation (2) for an aperture of 18.5 μm and a fluid density of 0.90 g/cm³ determined from tabulated pressure-volume temperature data for water (Kennedy and Holser, 1966).

Figure 6. Regression Fit

Resistivity

Fluid flow was halted for periods up to several days for both specimens and electrical resistance was monitored. For specimen DP 3916, fluid flow was halted for a period of 70 hours after 16 days of flow. The specimen was maintained at a constant temperature of 167°C during this time. Specimen DP 3972.2 was monitored under no-flow conditions for two intervals of approximately six days each: first at the beginning of the experiment prior to flow (Pre-Flow) and then at the end of the experiment after 27 days of flow (Post-Flow). A constant temperature of 167°C was maintained during the Post-Flow interval. Experimental conditions were more complicated during the Pre-Flow interval as confining pressure; pore pressure and the vessel temperature were raised in increments during the first three days of the experiment. Measured resistances declined from over 10 k Ω to under 2k Ω during this period. However, for comparison, only data from the latter part of the Pre-Flow period, when the specimen was at full confining and pore pressure

and at constant temperature, are shown in Figure 7. Normalized resistivity fell at a diminishing rate during each of the three no-flow intervals. The DP 3972.2 resistivity data are quite noisy during the no-flow intervals, but good results were obtained for specimen DP 3916.

Figure 7. Resistivity during no-flow intervals

A larger drop in resistivity was observed in the Pre-Flow interval than in the other two no-flow intervals. The larger resistivity response in the Pre-Flow interval is attributed to pore fluid contact with relatively fresh, unreacted rock surfaces. In the other two cases the fracture surfaces had been previously exposed to fluid flow for 16 days (DP 3916) or 32 days (DP 3972.2 Post-Flow). The fall in resistivity during no-flow intervals is interpreted as evidence that mineral dissolution on the fracture surfaces is releasing ions into the pore fluid, providing additional charge carriers. Much of the Desert Peak quartz monzonite is composed of potassium feldspar and plagioclase. Plagnes et al. (2000) observed abundant dissolution features in SEM photos of potassium feldspar and plagioclase mineral grains in crushed granite through which saline solutions had been flowed at 200°C. Chemical reactions between these minerals and water release a number of cations that would increase the ionic conductivity of the pore fluid (Table 2).

Equation (3) was found to provide very good fits to the smooth portions of resistivity data from each of the no-flow intervals

$$\rho = a + b \exp(-ct) + d \exp(-et) \quad (3)$$

where ρ is resistivity ($\Omega\text{-m}$), t is time (seconds) and a , b , c , d and e are fitting parameters. Two of the equation (3) fits are shown Figure 8 and the values of the fitting parameters are given in Table 3.

Figure 8. Fits to equation (3)

Electrical resistivity was observed to rise monotonically over time during periods of constant fluid flow for both specimens (Figure 9). The interval shown for specimen 3916 consists of the first 16 days of the experiment prior to the three-day cessation of flow on Day 16. Though not shown in the figure, resistivity continued to rise in specimen DP 3916 after flow was resumed. The experiment for specimen DP 3972.2 began with a no-flow interval of several days (the Pre-Flow interval). The DP 3972.2 resistivity data shown in Figure 9 are taken from the first 13 days of flow. The removal of dissolved ions downstream and by precipitation on the fracture surfaces is a likely cause for at least a portion of the rise in resistivity.

Figure 9. Resistivity during flow intervals

Conclusions

The experiments are at an early stage. The differential pressure measurements revealed an effective hydraulic aperture of 18.5 μm for specimen DP 3972.2. The electrical resistance measurements show that fluid resistivity rises (conductivity falls) during flow and falls during no-flow intervals. The fall in resistivity changes during the no-flow intervals is attributed a rise in ionic content of the pore fluid due to mineral dissolution. The fall in resistivity during flow may result from the loss of ions downstream (and out of the specimen) or from precipitation along the fracture surfaces.

Acknowledgements

D. Ruddle and W. Ralph prepared the samples and provided valuable technical assistance. S. Fletcher provided essential technical support. The cooperation of ORMAT and GeothermEx is gratefully acknowledged. This work was supported by the Office of Geothermal and Wind Technology, under the Assistant Secretary for Energy Efficiency and Renewable Energy of the U.S. Department of Energy, and the Office of Basic Energy Science, and was performed by University of California Lawrence Livermore National Laboratory under Contract W-7405-Eng-48.

References

- Clarke, S. P. Jr. (1966). "Viscosity" in Clarke, ed., Handbook of Physical Constants, Geol. Soc. Am. Memoir 97, Section 12, pp. 291-300.
- Detwiler, R. L., Roberts, J. J., Ralph, W. and Bonner, B. P. (2003). Modeling fluid flow and electrical resistivity in fractured geothermal reservoir rocks, *Proceedings, Twenty Eighth Annual Stanford Geothermal Reservoir Engineering Workshop, January 27-29, Stanford, CA*, SGP-TR-173, 301-306.
- Detwiler, R. L., and Roberts, J. J. (2003). Electrical resistivity as an indicator of saturation in fractured geothermal reservoir rocks: Experimental data and modeling, *Geothermal Resources Council 2003 Annual Meeting, Morelia, Mexico, October 12-15, 2003*.
- Kennedy, G. C. and Holser W. T. (1966). "Pressure-Volume-Temperature and phase relations of water and carbon dioxide," in Clarke, ed., Handbook of Physical Constants, Geol. Soc. Am. Memoir 97, Section 16, pp 371-383.
- Lutz, S. J. (2003). Summary of x-ray diffraction analysis, Energy & Geoscience Institute, University of Utah, Feb., 2003, 2 pp.
- Lutz, S. J., Schriener, A., Jr., Schochet, D. and Robertson-Tait, A. (2003). Geologic characterization of pre-tertiary rocks at the Desert Peak East EGS Project site, Churchill

Carlson, Roberts and Detwiler

County, Nevada, *Geothermal Resources Council 2003 Annual Meeting, Morelia, Mexico, October 12-15, 2003*.

Plagnes, V., Matsunaga, I., Azaroual, M., Tao, H., and Fujimoto, K. (2000). Granite-saline fluid interactions in a dynamic experimental system at 200 degrees C and 50 bars, *Proceedings, World Geothermal Conference 2000, Kyushu-Tohoku, Japan May 28 – June 10, 2000*, pp. 3829-3834.

Polak, A., Elsworth, D., Yasuhara, H., Grader, A. S., and Halleck, P. M. (2003). Permeability reduction of a natural fracture under net dissolution by hydrothermal fluids, *Geophysical Research Letters*, **30**, 2020-2024.

Roberts, J. J., Duba, A. G., Bonner, B. P., and Kasameyer, P. (2001). Resistivity during boiling in the SB-15-D core from The Geysers geothermal field: The effects of capillarity, *Geothermics* **30**, 235-254.

Robertson-Tait, A. and Morris, C. (2003). Progress and future plans at the Desert Peak East EGS Project, *Geothermal Resources Council 2003 Annual Meeting, Morelia, Mexico, October 12-15, 2003*.

Robertson-Tait, A., Lutz, S. J., Sheridan, J., and Morris, C. (2004). Selection of an interval for massive hydraulic stimulation in Well DP 23-1, Desert Peak East EGS Project, Nevada, *Proceedings, Twenty-ninth Workshop on Geothermal Reservoir Engineering, Stanford University*, V. 29.

Sanyal, S. K., Lovekin, J. W., Henneberger, R. C., Robertson-Tait, A., and Brown, P. J. (2003). Injection testing for an enhanced geothermal system project at Desert Peak, Nevada, *Geothermal Resources Council 2003 Annual Meeting, Morelia, Mexico, October 12-15, 2003*.

Sutopo, White, S. P. and Arihara, N. (2000). Modeling the evolution of granite permeability at high temperature, *Proceedings, World Geothermal Congress 2000, Kyushu-Tohoku, Japan, May 28 – June 10, 2000*, 2931-2936.

Table 1. Calculated changes in pressure differences across specimen for assumed initial fracture apertures

Aperture Reduction (μm)	Pressure Change (psi)	
	Initial Aperture 10 μm	Initial Aperture 20 μm
0	0.000	0.000
1	0.068	0.004
2	0.175	0.009
3	0.352	0.014
4	0.666	0.022
5	1.285	0.031
6	2.684	0.044
7	6.614	0.061
8	22.758	0.083
9	183.346	0.115

Table 2. Chemical reaction equations for major mineral components of Desert Peak quartz monzonite

Mineral	Comp. ¹ (%)	Reaction Equation ²
Quartz	7	$\text{SiO}_2 = \text{SiO}_2 (\text{aq})$
K-Feldspar	23	$\text{KAlSi}_3\text{O}_8 + 4 \text{H}^+ = \text{K}^+ + \text{Al}^{+++} + 3 \text{SiO}_2 (\text{aq}) + 2 \text{H}_2\text{O}$
Plagioclase (Albite)	44	$\text{NaAlSi}_3\text{O}_8 + 4 \text{H}^+ = \text{Na}^+ + \text{Al}^{+++} + 3 \text{SiO}_2 (\text{aq}) + 2 \text{H}_2\text{O}$
Plagioclase (Anorthite)		$\text{CaAl}_2\text{Si}_2\text{O}_8 + 8 \text{H}^+ = \text{Ca}^{++} + 2 \text{Al}^{+++} + 2 \text{SiO}_2 (\text{aq}) + 4 \text{H}_2\text{O}$

Sources: ¹Lutz, 2003. ²Sutopo et al., 2000.

Table 3. Resistivity curve-fitting parameters

Specimen	Duration (hrs)	a	b	c	d	e	R ²
DP 3916	70	17.41	1.368	6.164x10-5	4.832	5.855x10-6	0.9999
DP 3972.2 Pre-Flow	28.5	12.01	4.193	2.769x10-4	8.237	2.670x10-5	0.9992
DP 3972.2 Post-Flow	12.5	26.23	1.588	5.7668x10-5	1.540	5.6450x10-5	0.9989

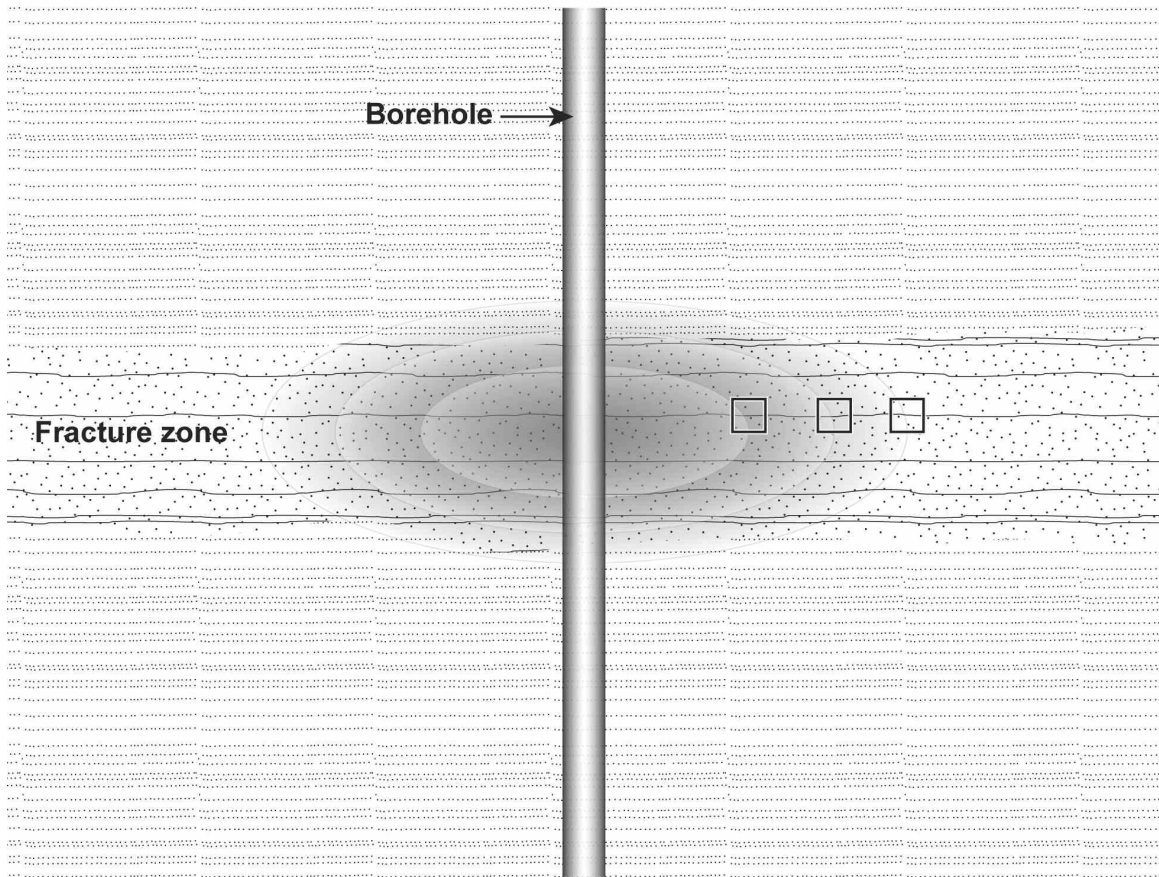


Figure 1. Schematic representation of a fractured injection zone at an EGS site. Water is injected at a rate over some interval. The injectate temperature is lower than the reservoir temperature. The shaded regions represent iso-temperature, chemical and fluid flux that change as a function of distance from the borehole. Our experiments are designed to test permeability evolution at a specific set of conditions (represented by the boxes in the fracture zone).



Fig. 2. Fracture surface of specimen DP 3792.2B, prepared by bead blasting. Magnification: 20x.

Carlson, Roberts and Detwiler

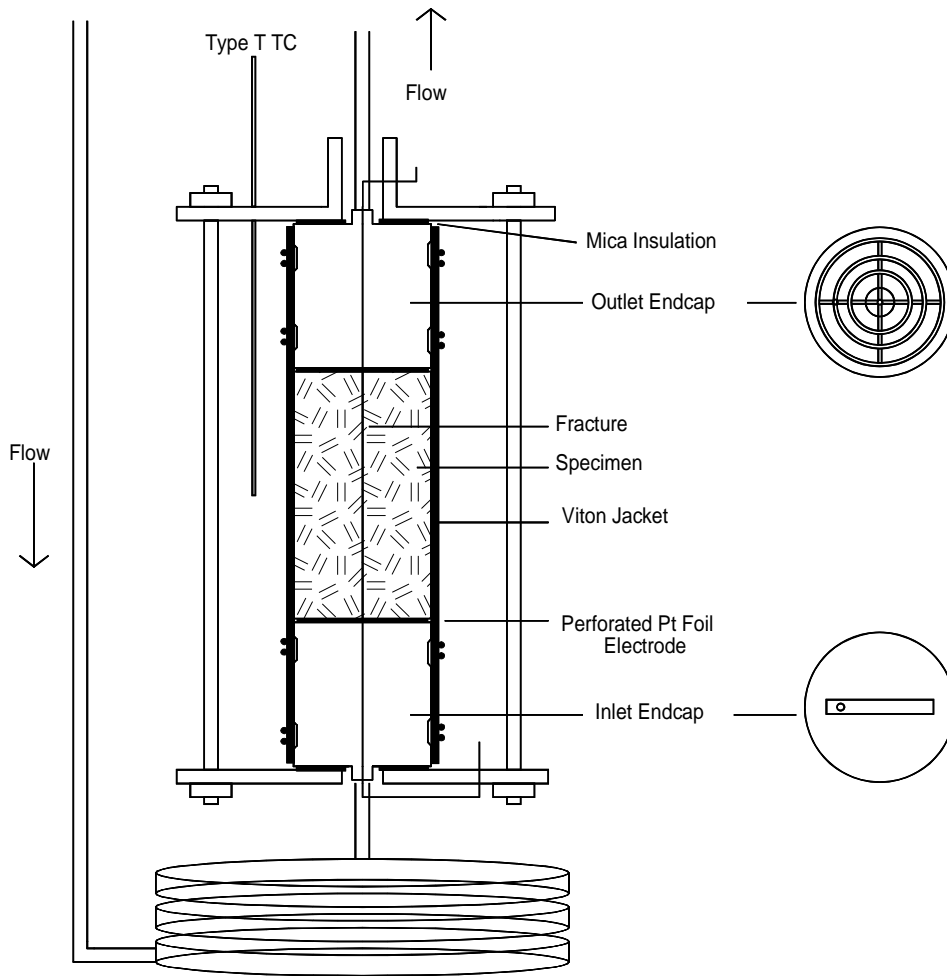


Fig. 3. Schematic diagram of specimen assembly. The inlet endcap contains a slot for distributing pore fluid to the fracture. The outlet endcap circular channels for collecting pore fluid. Resistance is measured with a pair of perforated platinum foil electrodes.

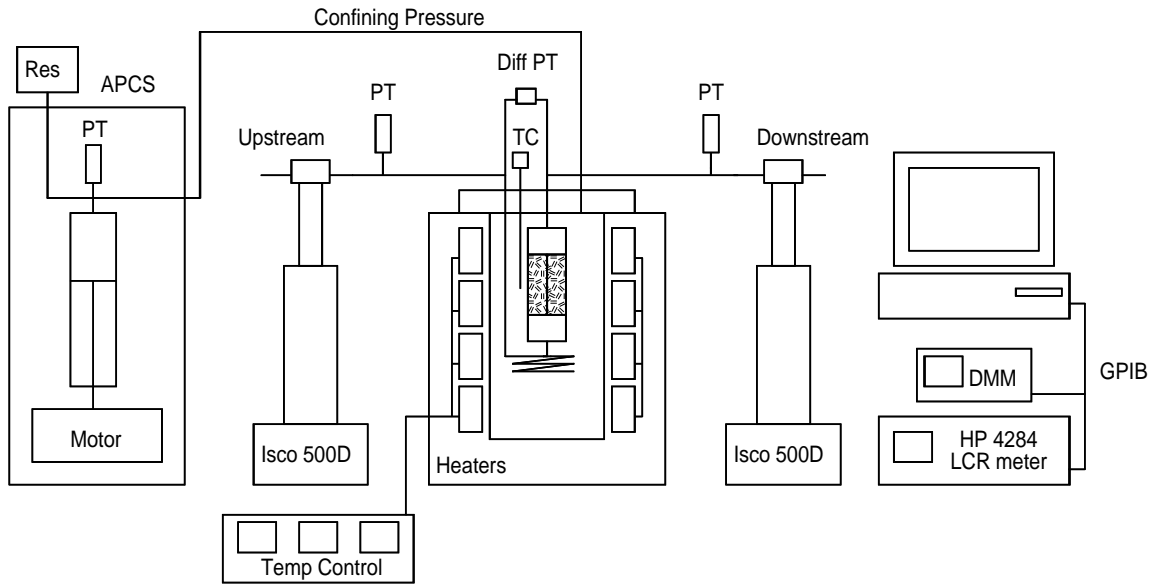


Fig. 4. Schematic diagram of experimental apparatus. The pressure vessel is externally heated. Confining pressure is supplied by an APCS pump under computer control. Upstream flow rate and downstream fluid pressure are controlled by Isco 500D syringe pumps. A Validyne DP-215 differential pressure transducer measures the fluid pressure drop across the specimen. An HP 4284A LCR meter measures electrical resistance across the specimen. Temperature is measured with a type-T thermocouple.

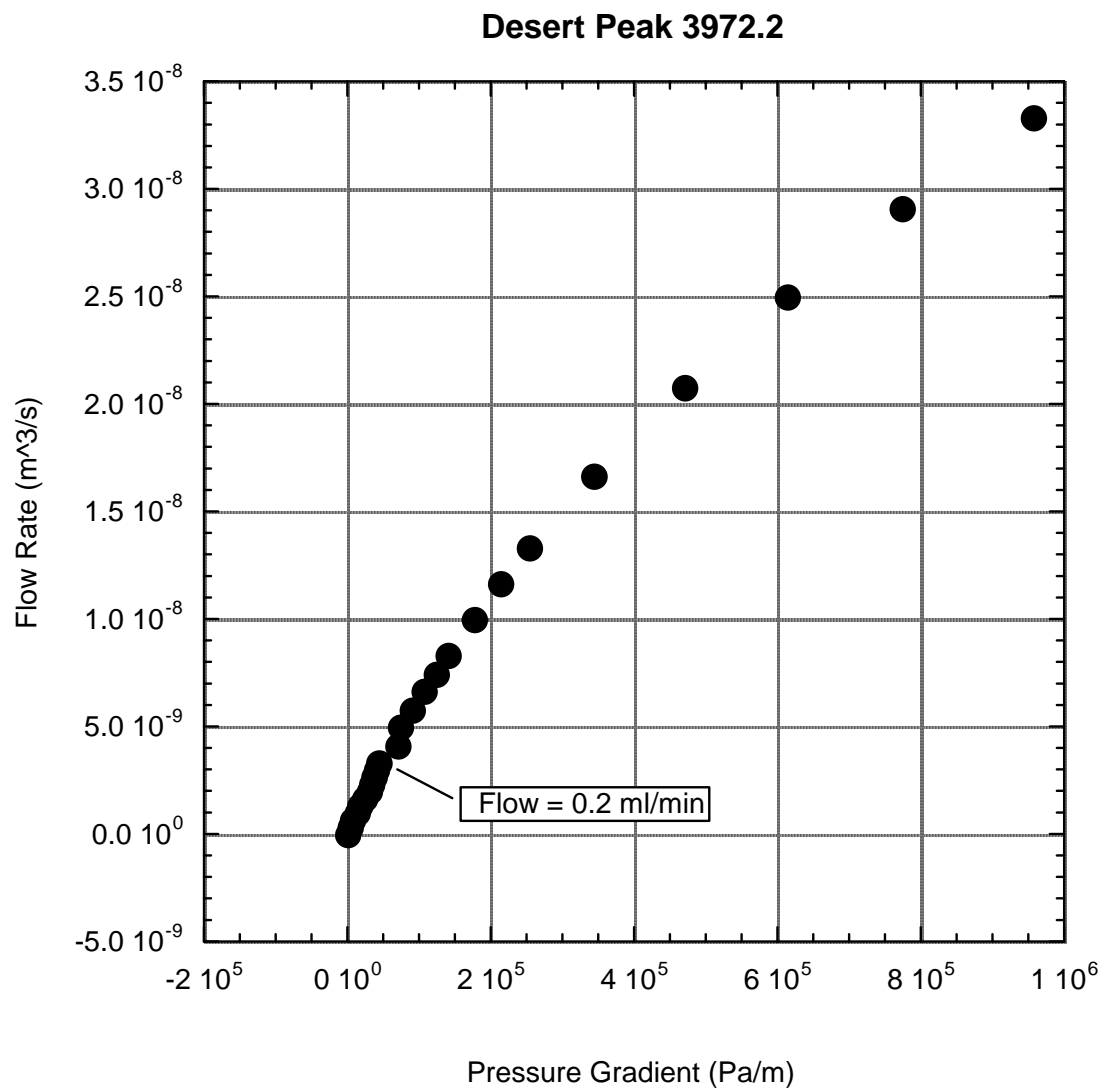


Fig. 5. Volumetric flow rate versus pressure gradient for specimen DP 3972.2 at flow rates between 0 and 2 ml/min. Nonlinearity is encountered at flow rates above 0.2 ml/min.

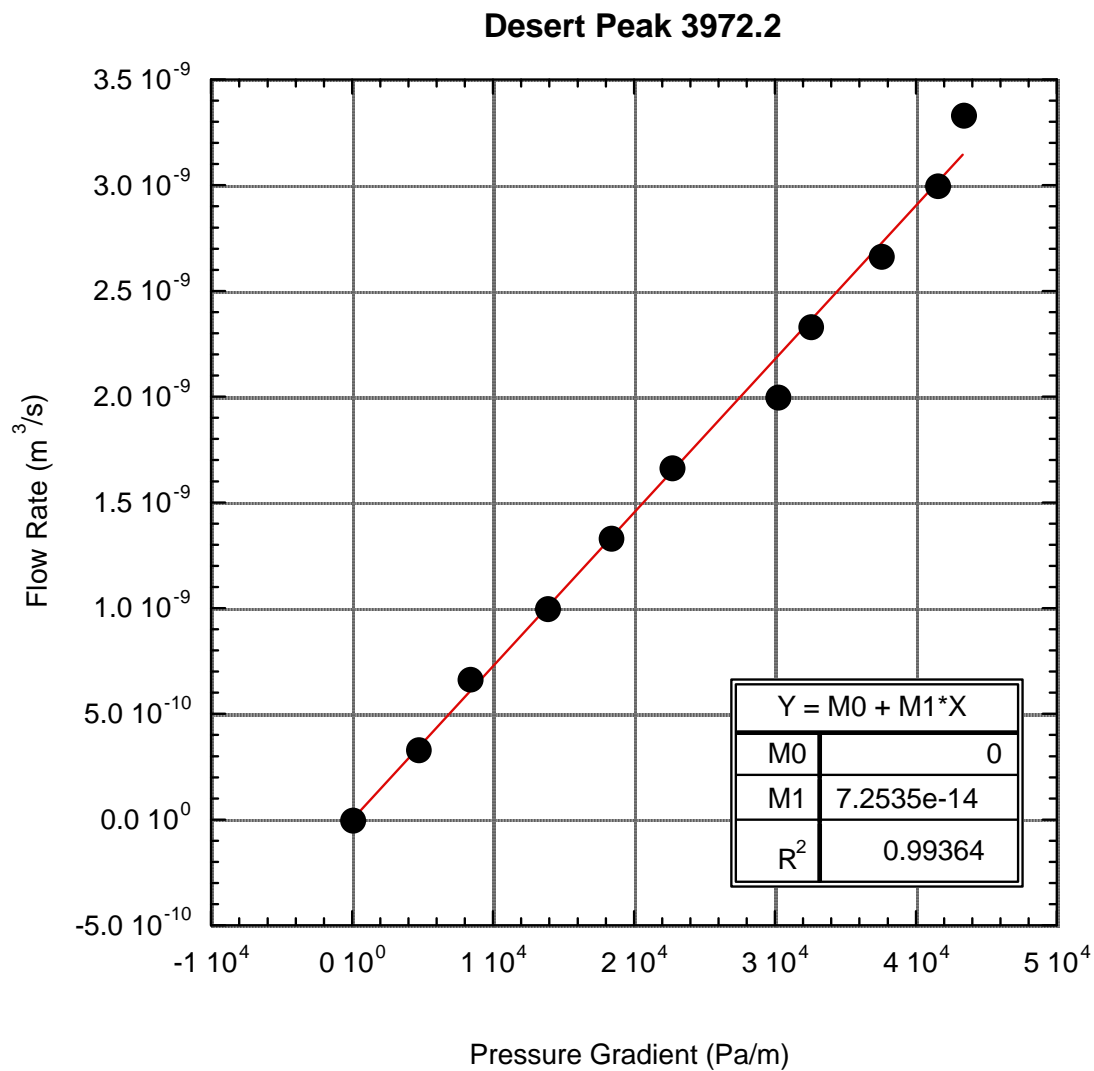


Fig. 6. Volumetric flow rate to 0.2 ml/min versus pressure gradient for specimen DP 3972.2. The regression line has been constrained to pass through the origin.

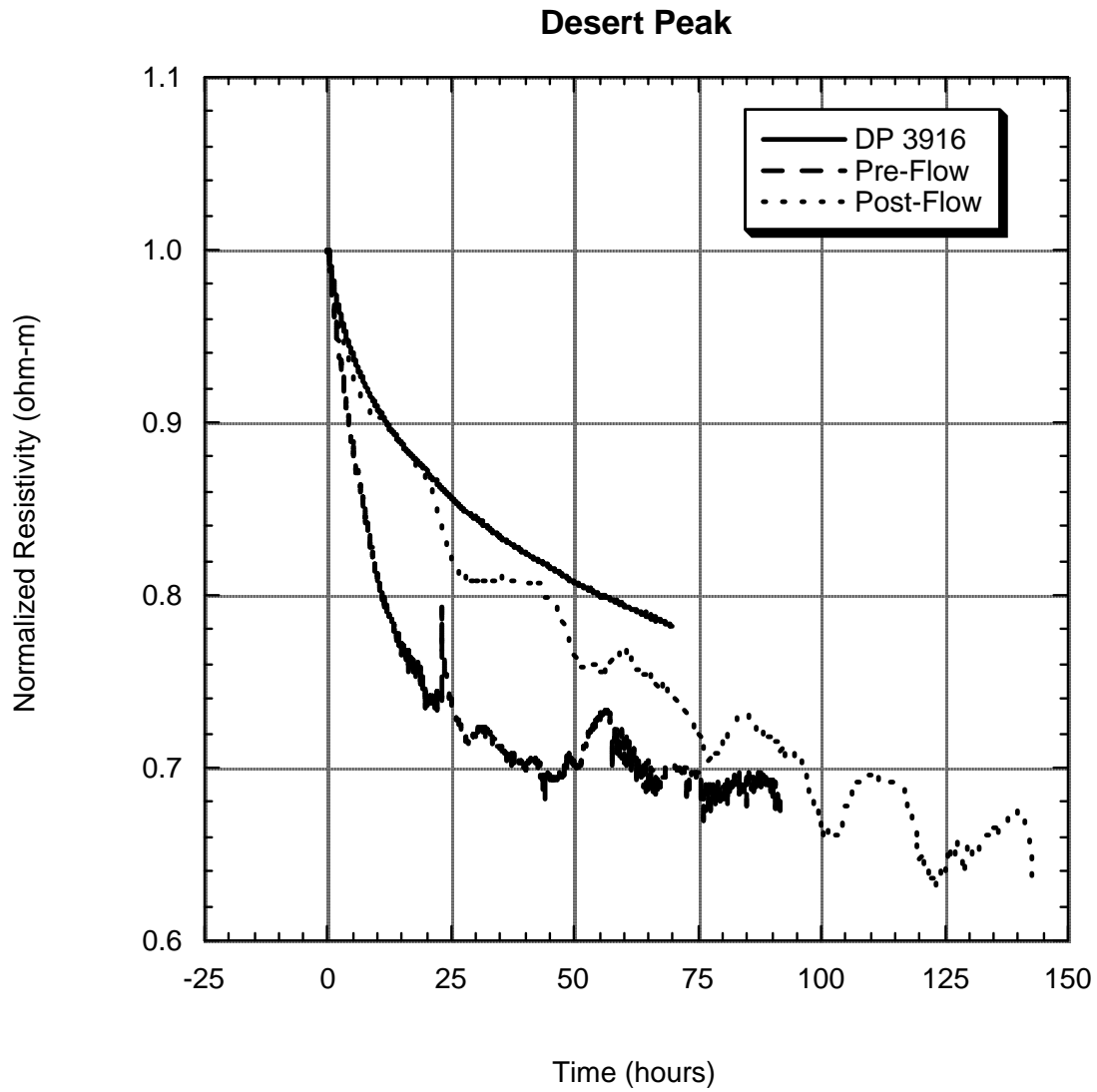


Fig. 7. Normalized resistivity during no-flow intervals for specimens DP 3916 and DP 3972.2 (Pre-Flow, Post-Flow). Resistivity dropped at a faster rate when pore fluid made contact with fresh fracture surfaces (Pre-Flow) than fracture surfaces that had previously been exposed to flow.

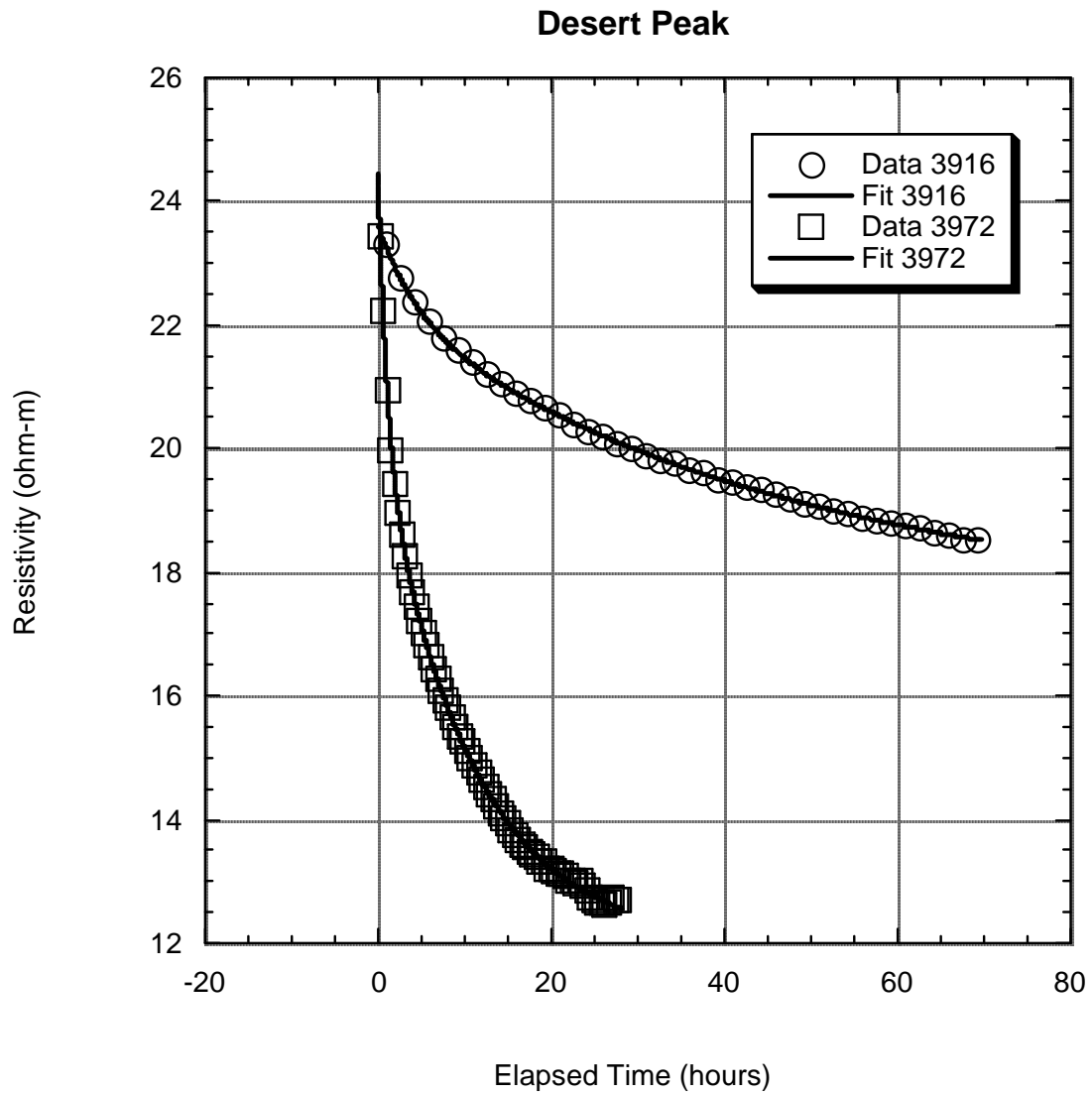


Fig. 8. Resistivity trends during no-flow intervals for specimens DP 3916 and DP 3972.2 (Pre-Flow). Solid lines are curve fits to equation (4). For clarity, only 2-5% of the data points are shown in the figure.

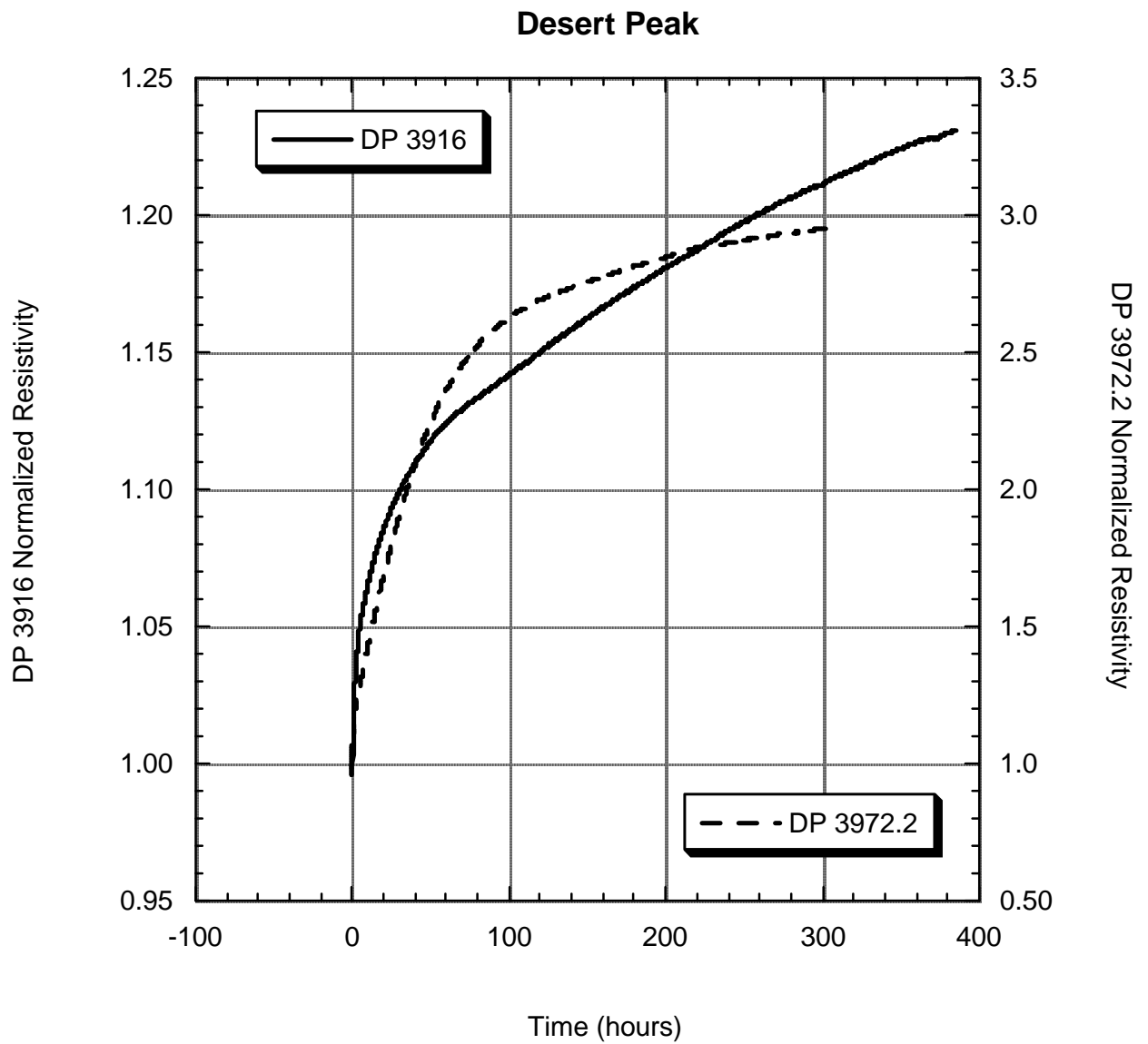


Fig. 9. Normalized resistivity during flow for Desert Peak specimens DP 3916 and DP 3972.2.